Morphology and Size Effect of Ceria Nanostructures on the Catalytic Performances of Pd/CeO2 Catalysts for Methanol Decomposition to Syngas

Morphology and size effect of ceria nanostructures on the catalytic performances of Pd/CeO_2 catalysts for methanol decomposition to syngas

Francesco Carraro,[§] Sunday A. Fapohunda,[§] Maria C. Paganini[#] and Stefano Agnoli[§]*

§ Università degli Studi di Padova, Dipartimento di Scienze Chimiche, Padova, 35122, Italy.

Università di Torino, Dipartimento di Chimica, Torino, 10125, Italy.

KEYWORDS: syngas; methanol; ceria; nanostructures; nanorods; nanocubes; nanoparticles; palladium.

ABSTRACT. Palladium is an active catalyst for the decomposition of methanol to syngas, and its chemical activity is largely affected by the interaction with the supporting substrate. Nanostructured Cerium oxide can establish strong electronic interactions with finely dispersed palladium nanoparticles (NPs) leading to a substantial enhancement of their catalytic performance.

To study this synergistic effect and connect it to structural parameters, we deposited Pd NPs on nanostructured cerium oxide particles exposing mainly the same (100) surface, but with different nanoshape and average dimension, and we have investigated their activity toward methanol decomposition reaction. A systematic comparison of photoemission measurements taken at every step of the catalytic cycle allowed us to identify the most important factors that control the redox properties of the Pd/CeO_2 systems and therefore the overall catalytic activity. Capitalizing on this knowledge it was possible to synthesize synergistic nanocatalysts with an excellent chemical activity at very low temperature.

INTRODUCTION.

Methanol decomposition to CO and H_2, i.e. syngas, is a quite interesting and versatile reaction that could be exploited in several catalytic processes[1], ranging from energy recovery of waste heat[2] (from various industrial activities[3] or from methanol fuel cells[4]) to the synthesis of fine chemicals.[5] Moreover, the *in situ* production of syngas is nowadays attracting a growing interest in catalysis, giving a "second youth" to the methanol decomposition reaction. In fact, if the catalyst used for syngas synthesis is rationally integrated in a more complex multifunctional material, the *in situ* produced CO and H_2 could be exploited to carry out a second catalytic reaction inside a tandem or cascade one-pot process.[5,6]

This approach could improve the overall safety and sustainability of a chemical transformation improving its energy efficiency and atom economy and minimizing waste and pollution. To achieve this ultimate goal however, it is necessary to improve the activity, selectivity and robustness of the catalytic centers. In the case of nanoparticle catalysts, these targets can be obtained by a careful design at the nanoscale of the size, morphology[7], and crystallographic

orientation of the facets of individual particles. A large body of literature works[8,9] demonstrates that these factors are essential to control both the surface chemistry of the nanoparticles as well as the chemical activity of a supported second phase.[10,11]

Palladium is extremely active in the catalytic decomposition of methanol to syngas and its activity is largely affected by the support, which in general is an oxide.[3,12,13] The reaction mechanism involves the dissociative chemisorption of methanol to form both a methoxy species and an surface hydride on the Pd surface. Then a sequence of oxidative dehydrogenation steps involving the hydrogen atoms attached to the carbon atom determines the formation of CO and other surface hydrides that recombine and desorb as molecular H_2.[14,15] Other authors although, suggested the possibility that methanol may be molecularly adsorbed and then undergo the cleavage of the C-O bond. This leads to the formation a series of CH_x intermediates and eventually to the deposition of coke.[16] More recently, it has been shown that both reaction paths are possible and the actual reaction conditions and nature of the catalyst (i.e. surface oxidation, exposed facets) dictate which of the two is favored.[17,18]

Cerium oxide is one of the most effective catalyst supports because it may strongly interact both chemically (e.g. oxygen spillover) and electronically (e.g. electron donation) with finely dispersed metal nanoparticles (NPs).[19,20,21] Some crucial properties of this oxide such as acid-base and redox properties are closely related to its surface structure. In fact, oxygen anions and cerium cations present different coordination and chemical environment according to their location on differently oriented low-index surfaces.[22,23,24,25,26] Therefore, controlling the morphology of ceria is a valuable tool to tailor the physicochemical properties of supported metal NPs and more in general the efficiency and selectivity of catalytic processes.[27,28,29] To shed light on the subtle links between structural properties and chemical activity we synthetized ceria NPs that mainly expose the same

{001} oriented facets, but that differ for the overall morphology (rods, cubes, polyhedral NPs) and physical dimension (2 nm to 20 nm). These substrates were then decorated with Pd NPs and their catalytic activity was investigated by using methanol as molecular probe. In the literature, most Pd/CeO_2 catalysts are prepared by impregnation[19~~15~~], coprecipitation[30] or deposition-precipitation[14,19~~15~~,31,32] methods, which all require a drastic thermal treatment to convert the Pd precursor to Pd NPs. In the present study, we investigated an alternative Pd deposition strategy that does not require a high temperature step. In fact, we deposited very small and finely dispersed Pd NPs by bubbling hydrogen in an aqueous dispersion of CeO_2 and K_2PdCl_4. After this step, our catalysts are ready to use and can be directly activated in the reactor. This procedure also has the additional benefit of preserving the initial morphology of the ceria supports, which was obtained by low temperature syntheses.

By combining a microscopic characterization via High-Resolution Electron Microscopy (HRTEM), Raman Spectroscopy, chemical investigation by *in situ* X-Ray Photoelectron spectroscopies (XPS), together with catalytic data obtained by gas chromatography, we were able to document the existence of a synergistic effect between ceria and palladium. This synergy is closely correlated with the morphology of the oxide support. Very small ceria NPs interact more strongly with Pd leading to formation of very small nanoparticles, which are characterized by a relevant faction of palladium oxides. Interestingly, *in situ* XPS demonstrated that in real catalytic (10 mbar CH_3OH) or reducing conditions (30 mbar H_2), the smaller is the dimension of the supporting oxide, the higher is its reducibility and its ability to promote the reduction of palladium NPs.

EXPERIMENTAL SECTION.

Synthetic procedures

Synthesis of CeO_2 small nanorods (SNRs)

Analytical grade $Ce(NO_3)_3 \cdot 6H_2O$ (Sigma Aldrich) and NaOH (WVR) were used as received. We followed the recipe reported by Pan et al. with little modifications.[33] Briefly, an amount of 15 ml of a 16 mM aqueous solution of $Ce(NO_3)_3 \cdot 6H_2O$ was mixed with 105 ml of a 14 M aqueous solution of NaOH in a Teflon beaker, vigorously stirred for 30 minutes and then left aging without stirring for 2 days at RT. The product was washed for 5 times with deionized water and dried at 60°C for 12 h.

Synthesis of CeO_2 nanocubes (NCs) and long nanorods (LNRs)

Analytical grade $Ce(NO_3)_3 \cdot 6H_2O$ (Sigma Aldrich) and NaOH (WVR) were used as received. We followed the synthesis protocol reported by Mai et al. with little modifications.[34] Briefly, an amount of 5 ml of a 0.15 M aqueous solution of $Ce(NO_3)_3 \cdot 6H_2O$ were mixed with 10 ml of a 9 M aqueous solution of NaOH in a 25 ml Teflon-lined stainless steel autoclave. The autoclave was left in an oven at 180°C (for NCs) or 110°C (LNRs) for 24 h. The product was washed for 5 times with deionized water and dried at 60°C for 12 h.

Deposition of Pd nanoparticles

To prepare a catalyst loaded with a 5% Pd weight percentage in the final material, we mixed 30 mg of K_2PdCl_4 (Sigma Aldrich) and 198 mg of CeO_2 (nanoparticles, nanorods, nanocubes or commercial nanopowder (CNPDs) from Sigma Aldrich) in 100 ml of deionized water. Under vigorous stirring at RT, we bubbled a 2:1 N_2:H_2 flow for 30 minutes. Finally, the product was washed for 5 times with deionized water and dried at 60°C for 12 h.

Physicochemical characterization

X-ray photoemission spectra were acquired using a conventional x-rays source (1486.6 eV photons). The measurements of the as-prepared materials were taken after a short annealing at 150°C in UHV to remove most adsorbed species (water and contamination debris). The calibration of the binding energy (BE) scale was determined using the C 1s photoemission line of adventitious carbon as reference. The photoemission lines were separated into individual components (after Shirley background removal) using symmetrical Voigt functions and non-linear least squares routines for the χ^2 minimization. *In situ* XPS measurements were performed employing a custom-made high-pressure cell (base pressure: 10^{-7} mbar) connected to the analysis chamber. After the analysis of the as-prepared catalyst, the sample was transferred in the high pressure cell and exposed in static conditions to i) hydrogen, 30 mbar, 1h and to ii) methanol, 10 mbar, 30 min at 300°C. After each step, the sample was transferred back in the analysis chamber in ultra-high vacuum and the photoemission spectra were acquired.

The nano- and micro-scale morphology of materials was investigated by HR-TEM. HRTEM micrographs were acquired using a Jeol JEM 3010 (300kV) microscope equipped with an EDS detector by Oxford Instruments.

Characterization by Raman spectroscopy was performed using a ThermoFisher DXR Raman microscope. The spectra were recorded using a laser with an excitation wavelength of 532 nm (1 mW), focused on the sample with a 10× objective (Olympus). Raman peak shifts and areas were determined by fitting with Lorentzian lineshapes ($R^2 > 0.95$).

The specific surface area was measured applying the single-point BET method, using a Micromeritics ASAP 2020 instrument.

Evaluation of the catalytic activity

The catalytic activity toward methanol decomposition was evaluated in a fixed-bed continuous-flow quartz reactor (inner diameter: 4mm) under atmospheric pressure. The catalyst powder (20 mg) was dispersed in quartz wool and activated in a flow of 20 vol% hydrogen diluted with argon (total flow-rate: 50 sccm) for 1 h at 300°C. Then the sample was cooled to RT and 1 vol% of methanol was fed with an argon carrier (total flow-rate: 50 sccm; weight hourly space velocity: 1500 ml h^{-1} g-cat^{-1}) at different temperatures (from RT to 350°C). The outlet gas was analyzed with an on-stream gas chromatograph (Agilent 490 microGC) equipped with a Molsieve 5A, a CP-WAX 52 and a PORAPLOT-U columns (10 meters) for gas separation and a thermal conductivity detector. The temperature was stabilized for 15 minutes before every acquisition.

RESULTS AND DISCUSSION.

CeO_2 nanocubes (NCs), small nanorods (SNRs) and long nanorods (LNRs) were synthesized following previously reported recipes with little modifications. These materials were compared with commercially available CeO_2 nanopowders (CNPDs). All four nanostructured oxides were decorated with Pd NPs (5% weight): the different CeO_2 powders were dispersed in an aqueous solution of K_2PdCl_4, and then molecular hydrogen was bubbled in the solution at RT to reduce the salt and deposit Pd NPs. The amount of Pd was determined by EDS and confirmed the quantitative deposition of Pd (5% weight). Moreover, both XPS and EDS data indicated that the washing procedure after metal deposition did not leave impurities of NaOH or unreacted Pd precursor (no signals ascribable to Na, K or Cl were observed).

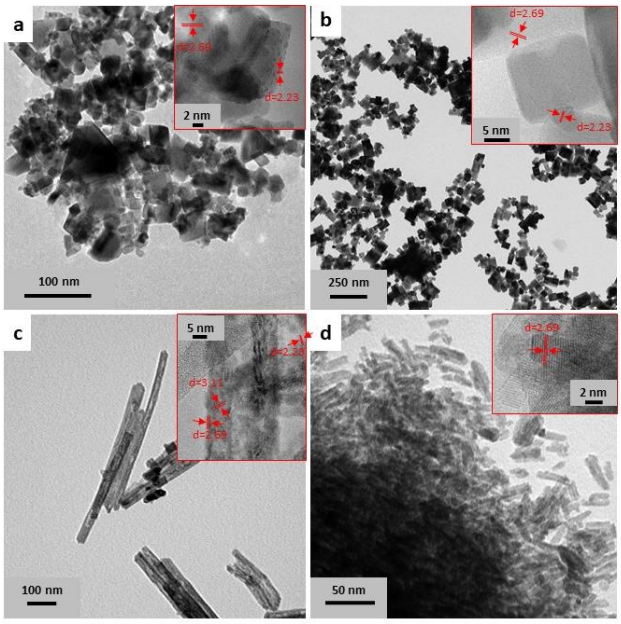

Figure 1. TEM and HRTEM (insets, highlighted interplanar distances (d) are reported in nm) micrographs of as prepared 5%wt Pd/CeO_2 CNPDs (a), 5%wt Pd/CeO_2 NCs (b), 5%wt Pd/CeO_2 LNRs (c) and 5%wt Pd/CeO_2 SNRs (d).Figura da modificare

The morphology of the ceria samples and their decoration by Pd NPs were studied by TEM and HR-TEM (Figure 1, and S1-7)). The CeO_2 CNPDs show a wide size distribution (mainly 10-20 nm), variable morphology and expose mainly {100} and {111} oriented facets (Figure 1a, S7). On the contrary, CeO_2 NCs consistently present highly crystalline cubic nanoparticles terminating with {100} oriented surfaces and exhibit an average size of 16-20 nm (Figure 1b, S6). From TEM micrograph, the CeO_2 SNRs exhibit a slightly elongated shape with dimensions along the minor axis of about 3-5 nm and more variable along the larger axis of about 10-30 nm. (Figure 1d). They tend to aggregate, however, by carefully analyzing HR-TEM micrographs, we verified that the SNRs are composed by rather crystalline nanoparticles. From lattice fringe analysis, it may be deduced that all the NPs expose mainly {100} facets (Figure S4). Therefore, the SNRs can be described either as nanorods characterized by a low aspect ratio, or as cubes that became slightly

elongated in one direction. The CeO_2 LNRs have a uniform width of 10±2 nm and a length ranging from 900 to 250 nm (Figure 1c). The long sides of the rod expose {100} surfaces, whereas the transversal basal faces are {111} oriented (Figure 1c, S5). Pd NPs are finely dispersed over the different substrates and their size is ranging from 3 to 5 on CNPDs, from 2 to 10 nm on NCs and LNRs, and expose mainly (111) facets (Figure S1-3 and S5-7). In the case of CeO_2 SNRs, the Pd NPs are exceedingly small ~~(<2 nm)~~ and because of that it was not possible to define clearly their size distribution. Nevertheless the presence of Pd also on these samples has been certified by the EDX analysis, in fact a concentration of Pd around x% has been found.

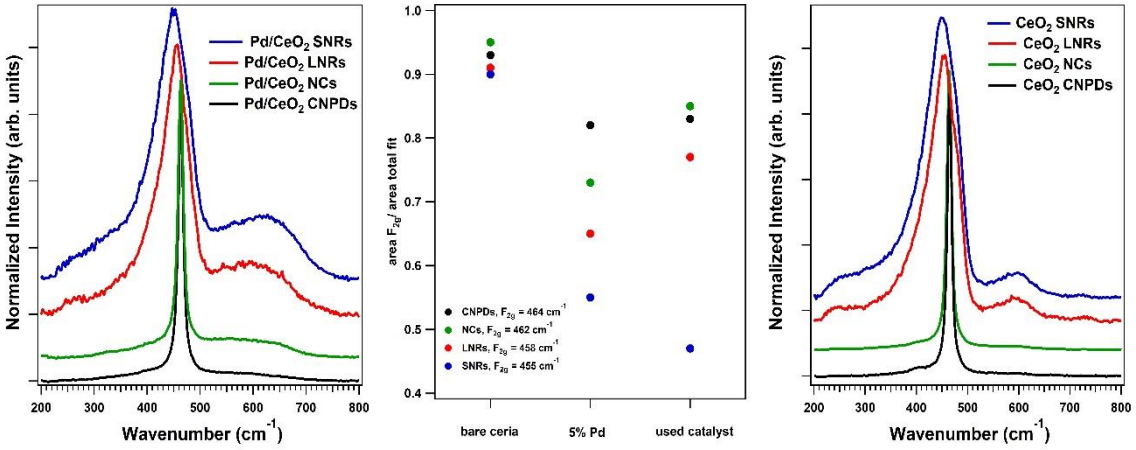

Figure 2. Raman spectra of as-prepared bare (right) and 5%wt Pd decorated (left) CeO_2 CNPDs, NCs, LNRs and SNRs and the results of the fitting of Raman spectra in the region 300-800 cm^{-1} for these samples (center).

The Raman spectra of CNPDs NCs, SNRs, LNRs are shown in Figure 2. All samples show the first-order F_{2g} peak typical of CeO_2 at about 465 cm^{-1}, confirming the formation of the fluorite phase. The Raman shift and the half-width at half-maximum (FWHM) of the F_{2g} peak depend on the particle size[35,36] and their trend confirms the results of TEM investigations. As expected, the F_{2g} peak of SNRs shows the lowest Raman shift (455 cm^{-1}) and the highest FWHM (60 cm^{-1}), and conversely commercial CeO_2 F_{2g} peak exhibit the highest Raman shift (464 cm^{-1}) and the smallest

FWHM (8 cm^{-1}). Moreover, a weak peak around 600 cm^{-1}, which is usually associated with defects (i.e. oxygen vacancies in CeO_2)[36~~32~~] can be observed in all powders. Based on the relative intensity of this peak, the SNRs present the highest oxygen vacancies concentration, whereas CNPDs the lowest. After the Pd NPs deposition, the intensity of such peak increases in all the investigated samples. This may be associated with an interfacial reaction between Pd and CeO_2, which leads to the reduction of this latter (Figure 2).[36~~32~~,37] In SNRs and LNRs this effect is stronger than in CNPDs and NCs. Therefore, overall Raman results highlight the higher reducibility of SNRs and LNRs compared to NCs and CNPDs.

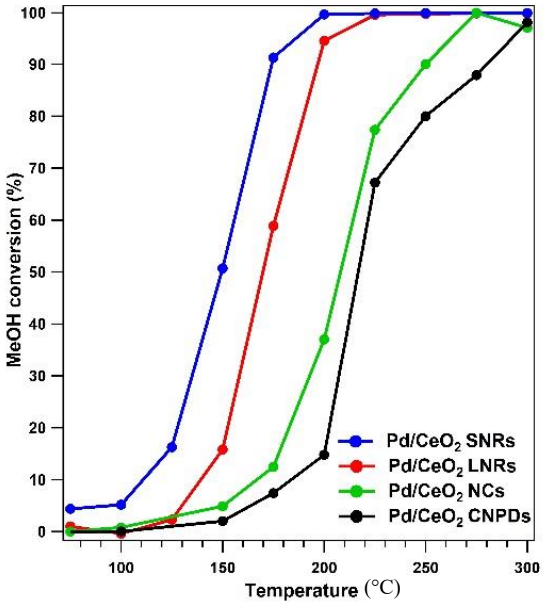

Figure 3. Methanol conversion vs temperature for the catalysts activated at 300°C in H_2.

The catalytic activity toward methanol decomposition was studied in the temperature range between 100°C and 350°C in a fixed-bed continuous-flow (1% vol of CH_3OH, 1500 ml h^{-1} g-cat^{-1}) quartz reactor under atmospheric pressure after activating the catalysts with hydrogen (300°C, 1h, 20% of H_2 in Ar). The gas stream out of the reactor was analysed by an on-stream gas chromatograph. The main results of chemical conversion are summarized in Table 1 and Figure 3.

The activity of 5 wt% Pd/CeO_2 SNRs is always higher than that of the other Pd/CeO_2 catalysts in the temperature range between 100-350°C. All Pd/CeO_2 nanostructures showed an extremely selective methanol decomposition to CO and H_2, as the best-performing Pd/CeO_2 catalysts reported in the literature.[13,14] Other products marginally detected are CH_4 and CO_2. CO_2 (Selectivity <0.5 %) was observed mainly at temperature lower than 200°C; conversely, CH_4 was detected at T>275-350°C in the case of CNPDs and NCs, and between 225 and 350°C in the case of SNRs and LNRs. It is worth mentioning that, in absence of Pd nanoparticles, the bare CeO_2 substrates exhibit a rather scarce chemical activity, starting to convert methanol only above 200°C.

Table 1. Catalytic results and BET surface area of the investigated materials.

Catalyst	BET surface area (m^2/g)	T_{50} (°C)[a]	T_{100} (°C)[b]	Selectivity (%) at T_{100}	
				CO	H_2
$5\%_{wt}Pd/CeO_2$ CNPDs	60	220	300	99.5	99.7
$5\%_{wt}Pd/CeO_2$ NCs	35	205	275	99.6	98.3
$5\%_{wt}Pd/CeO_2$ LNRS	95	175	225	88.0	99.8
$5\%_{wt}Pd/CeO_2$ SNRs	150	150	200	99.8	99.9
Notes	[a] Temperature of 50% methanol conversion [b] Lower temperature of 100% methanol conversion				

Regarding the activity of the catalyst, the temperature of 50% methanol conversion (T_{50}) is usually a standard benchmark. In the case of $5\%_{wt}Pd/CeO_2$ SNRs, we obtained a value of 150°C.

Moreover, by the analysis of chemical conversion vs temperature we estimated an activation energy for methanol decomposition of 38 kJ/mol in the temperature range between 125 and 175°C, which nicely compares with the value of about 70-80 kJ/mol reported for Pd NPs supported on different metal oxides.[38~~34~~] For the other catalytic systems, the T_{50}s of $5\%Pd/CeO_2$ LNRs, NCs and

CNPDs is 170°C (43 kJ/mol, 150-200°C), 205°C (51 kJ/mol, 175-225°C) and 220°C (58 kJ/mol, 200-250°C). All data are summarized in Table 1.

Overall, the catalytic activity of 5%Pd supported on CeO_2 SNRs and LNRs is excellent. To the best of our knowledge, it is higher than most of previously reported CeO_2 supported Pd catalysts (i.e. 17% wt Pd/CeO_2: T_{50}=200°C; 5% Pd deposited on mesoporous CeO_2: T_{35}=180°C; 3 wt% Pd/CeO_2: T_{50}=174°C)[3,13, 14] and of other metal/metal oxide catalysts (3 wt% Pt/CeO_2: T_{50}=158°C; 3 wt% Pt/Al_2O_3: T_{50}=182°C)[14].

In general, the different catalytic performances of ceria based systems can be associated with the type of exposed surfaces, the different defectivity (concentration of oxygen vacancies) and reducibility of the solid. In fact, the adsorption of methanol on ceria depends on the formation of methoxy and hydroxyl species.[22~~18~~,29~~25~~] These species are more stable on CeO_2 surfaces with a stronger basicity of O anions. Clear surface structure dependence was found for the strength and amount of base sites: (110) > (100) > (111).[22~~18~~,24~~20~~] Moreover, this tendency is strengthened under reductive reaction conditions and corresponds well to the trend of the energy of oxygen vacancy formation.[22~~18~~,24~~20~~] In the investigated nanopowders, the main exposed facets are the {100}. Interestingly, the worst performing material is Pd/CNPDs, which exhibits the highest abundance of {111} facets (about 1/10 with respect to {100} facets). However, nanorods also exhibit some limited amount of {111} faces but they are extremely active, therefore other factors may be at play.

In order to shed some light on the surface chemistry and Palladium/Ceria synergies that may be responsible for this excellent activity and to rationalize the differences observed in our set of catalytic systems, we systematically applied X-ray photoemission spectroscopy (XPS) and in particular *in situ* XPS, which allows investigating the surface of our catalysts in working

conditions, without exposing the materials to the atmosphere. This has been done at each steps of the catalytic process, i.e. for the as-prepared catalyst, after activation and after working conditions. This analysis provided a detailed insight into the Pd oxidation state and the redox properties of the CeO_2 substrates that could be related to the different catalytic activities. Moreover, these results were compared with the data acquired from the same experiments performed on the bare CeO_2 nanostructures to assess the effect of Pd on the redox properties of CeO_2.

The results of the separation into chemically shifted components of Ce 3*d* and Pd 3*d* photoemission lines are summarized in tables 2, 3 and S1, and reported in Figures 4, S9 and S10. The photoemission spectrum of Ce3*d* was fitted with the five typical spin-orbit-split doublets that correspond to the possible 3*d*4*f* configurations in the photoemission final state. The components labeled v^0 and v^i corresponds to Ce^{3+}, whereas the components labeled v, v^{ii}, v^{iii} corresponds to Ce^{4+} (Figure 4a).[38,39,40,41,42] The spin-orbit-split satellite labeled u^{iii} centered at 917 eV is distinctive of the poorly screened Ce3$d^9$4f^0O2p^6 final state, and is connected only with the presence of Ce^{4+} ions. For this reason, to follow the reduction degree of the CeO_2 surface, we reported in table 2 the ratio of the area of the u^{iii} component versus the total area of the fit Ce3*d* photoemission line and in table S1 we show the complete results of the analytical fitting. Therefore, a lower value of this parameter corresponds to a higher reduction of CeO_2 surface. This procedure limits the uncertainty introduced by the fitting procedure. The data reported in Tables 2 and S1 indicate that the most reduced samples are the SNRs (65% of Ce(III) in the case of activated Pd/SNRs sample), whereas all the other systems present a very similar reduction degree. This is in good agreement with the Raman Spectroscopy data and supports the idea that the major factor affecting the reduction properties of CeO_2 is related to the physical dimension.[11,43,44]

Pd 3*d* photoemission lines were fitted employing three spin-orbit-split doublets corresponding to the Pd oxidation states 0, II and IV. Pd(II) and Pd(IV) were fixed at a binding energy (BE) of 336.7 and 338.2 eV, respectively (Figure S9).

Table 2. Summary of the separation into chemically shifted components of Ce3d photoemission lines of Pd/CeO_2 catalysts as-prepared, activated (H_2) and after exposure to methanol in working conditions (MeOH).

	Ce3*d* fit results: (area u[iii])/(area of total fit)							
	SNRs		LNRs		NCs		CNPDs	
	bare	5% Pd	bare	5% Pd	bare	5% Pd	bare	5% Pd
asprepared	0.080	0.072	0.095	0.08	0.092	0,089	0,100	0,092
H_2	0,078	0,042	0,07	0,052	0,094	0,078	0,089	0,087
MeOH	0,051	0,05	0,066	0,055	0,089	0,082	0,087	0,088

Table 3. Summary of the separation into chemically shifted components of Pd3d photoemission lines of bare CeO_2 and Pd/CeO_2 catalysts as-prepared, activated (H_2) and after exposure to methanol in working conditions (MeOH).

	Pd3*d* fits results: area %											
	SNRs			LNRs			NCs			CNPDs		
	Pd(0) 335,9 eV	Pd (II)	Pd (IV)	Pd(0) 335,55 eV	Pd (II)	Pd (IV)	Pd(0) 335,4 eV	Pd (II)	Pd (IV)	Pd(0) 335,6 eV	Pd (II)	Pd (IV)
asprepared	0,30	0,17	0,51	0,28	0,20	0,52	0,24	0,27	0,49	0,38	0,42	0,2
H_2	0,91	0,09	0	0,59	0,36	0,05	0,75	0,25	0	0,84	0,16	0
MeOH	0,87	0,13	0	0,69	0,25	0,06	0,76	0,24	0	0,85	0,15	0

Conversely, the energy position of the Pd(0) component was allowed to vary slightly because it could be influenced by the size of the nanoparticles and by the electronic interaction with the ceria substrates. In fact, many studies reported a strong effect induced by the oxide substrate on the valence of Pd: the interaction of the metal NPs with the oxide support leads to an electron transfer

from Pd to ceria and to the formation of interfacial Pd cationic species. [30~~26~~,14,45] Interestingly, the presence of Pd species with valence close to +1, identified by an upward BE shift of about 0.5 eV with respect to the typical position of metal Pd $3d_{5/2}$ (335.0 eV), correlates well with an enhanced catalytic activity toward methanol decomposition.[30~~26~~,14] The reason for this enhanced activity is not fully understood in the literature, but it is thought to be connected with a change in the surface stabilization of CO. On the one hand cationic Pd species interact with CO less strongly than the metal preventing the poisoning of the active phases, on the other hand they can activate CeO_2 that becomes able to adsorb CO at much lower temperature.[19]

As demonstrated by HR-TEM micrographs, the smallest Pd NPs are deposited on CeO_2 SNRs, whereas the largest ones on CeO_2 NCs and LNRs (about 2-10 nm). The Pd $3d_{5/2}$ peak maximum in metal Pd is usually reported at 335.0 eV. Because of the so called "small cluster size effect",[46,47] the Pd(0) component of the Pd NPs on CeO_2 SNRs (335.9 eV, Figure S9a) shows the largest shift toward higher BE with respect to the other samples (Figure S9b-d).[48] The different catalysts also show a different amount of oxidized species Pd(II) and Pd(IV), which correlates well with the dimension of the Pd NPs especially in the case of the Pd(IV) components. This suggests that small NPs can be more efficiently oxidized by the ceria substrate forming a more relevant partially oxidized interface, and consequently a more extended reduction of the CeO_2 surface.[40~~36~~] However, the differences in the BE of Pd(0) components may not only be associated with the size of the Pd NPs. In fact, in the case of LNRs and NCs the size distribution of Pd NPs is similar and the higher BE of Pd(0) of LNRs (335.55 vs 335.4 eV) could be associated with a stronger electronic interaction between Pd and the CeO_2 support.[19~~15~~,45~~41~~] This hypothesis is also sustained by considering the effects of Pd deposition on the reduction degree of CeO_2. In fact, the decoration of Pd NPs influences in different ways the oxidation degree of the various CeO_2 substrates, as

demonstrated also by the previously discussed Raman Spectroscopy data. CNPDs and NCs Ce3*d* photoemission lines show only a slight increase of the $Ce^{3+}/(Ce^{3+}+Ce^{4+})$ ratio after Pd deposition (Figure 4c,d and S8c,d; from 25% to 27% and from 30% to 31%, respectively). On the contrary, the most evident changes in CeO_2 oxidation degree are visible in LNRs and SNRs (Figure 4a,b and S8a,b; Ce^{3+} from 29% to 35% and from 33% to 38%, respectively). Especially in the case of LNRs, the CeO_2 support is heavily reduced after the Pd deposition, highlighting the strong Pd-CeO_2 interaction.

After activation in hydrogen atmosphere (300°C, 30 mbar, 1h), all the catalysts were reduced considering both the oxide support and the supported metal nanoparticles. The Pd NPs are almost totally reduced to metal Pd in all cases (Figure S9). However, the largest fraction of reduced Pd is found on the NPs deposited on SNRs. Quite surprisingly, the most relevant amount of oxidized Pd is observed on LNRs. This may seem an unusual result considering their close structural relationship with SNRs that have an opposite behavior. This apparent contradiction can be explained by the different size of Pd NPs: the extremely small NPs on SNR are extremely reactive and kinetically fast to respond to variations in the gaseous environment, whereas the bigger NPs supported on the LNRs are kinetically hindered and pinned by the already mentioned strong interaction with the substrate. Moreover, after activation in hydrogen, the most reduced CeO_2 supports (either with or without Pd) are SNRs, followed by LNRs and then by NCs and CNPDs. This suggests that both types of nanorods are easier to reduce with respect to other ceria nanoshapes. While this enhanced reducibility could be associated with the small dimension in SNRs, such explanation would fail in the case of LNRs. On the other hand, both samples were prepared in the lowest temperature conditions, therefore we can deduce that some structural defects intrinsic to their synthesis may be responsible for the facilitated reduction. Moreover, as

demonstrate by BET measurements (see table 1), both type of nanorods exhibit the highest surface area and therefore the highest number of low coordination sites among the different supports, which may favor an enhanced reduction operated by reacting with a reducing gas phase

The analysis of the Pd 3*d* and Ce 3*d* spectra after exposure to methanol (300°C, 10 mbar, 30 min), indicates that the CNPDs, NCs and LNRs are almost unchanged (Figures 4, S8 and S9) with respect to the H_2 treatment only, evidencing a small reduction or oxidation of Ceria in presence or absence of Pd, respectively. In the case of SNRs, after methanol exposure, the metal free NPs undergo a significant increase of the Ce 3*d* (III) component, whereas on the metal decorated substrates the trend is reversed. This slight oxidation of CeO_2 may be associated with the higher local concentration of CO (Figure S4a,b) that can eventually leave a surface carbon layer, which can be hydrogenated to CH_4 at the investigated temperature while residual oxygen restore the surface O vacancies.[32~~28~~,49,50] This effect is more significant in Pd/SNRs, which is the most active materials with the lowest $T_{50.}$

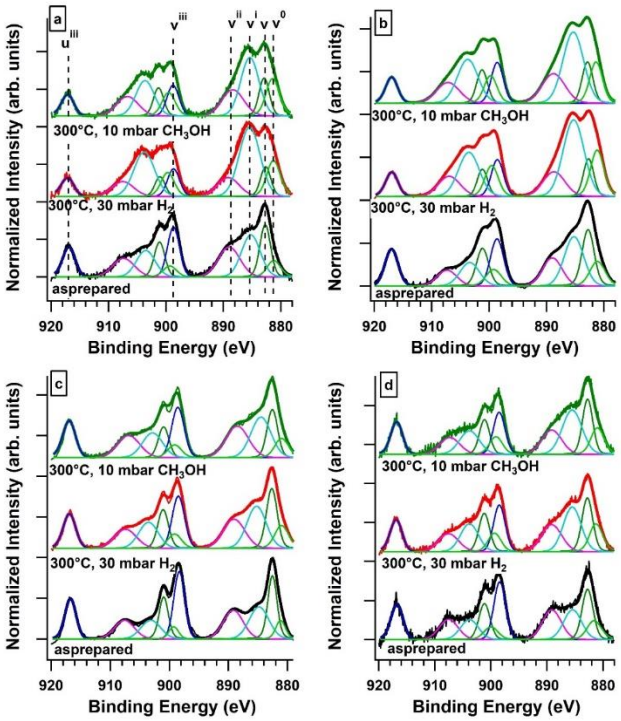

Figure 4. Ce3d photoemission lines, as well as the separations into single chemically shifted components, of a) 5%wtPd/CeO_2 SNRs, b) 5%wtPd/CeO_2 LNRs, c) 5%wtPd/CeO_2 NCs and d) 5%wtPd/CeO_2 CNPDs of as prepared, activated and after exposure to methanol in working

In conclusion, the XPS data suggest that Ceria in form of SNRs is extremely responsive to the change of the gaseous environment due to the small dimensions and consequent strong interaction between the oxide substrate and supported metal. A similar behavior is observed also for LNRs, but in this case the reduction level of Pd remains lower because of the larger NP dimension. Anyway, in both types of nanorods it is observed the highest synergistic effect between Pd and CeO_2 as demonstrated by the strong reduction of ceria after the H_2 treatment in the systems decorated by Pd compared to those without. Interestingly, even if they expose the facets with the lowest oxygen formation energy (i.e {100}) with respect to LNRs that expose also a small part of {111} surfaces, NCs do not reach the same amount of reduction in reducing conditions (either in CH_3OH or H_2) as the two different types of nanorods. This is probably due to their larger size,

higher crystallinity and absence of defects, which are a consequence of their higher synthesis temperature.

The influence of the exposed facets is predominant for the two catalysts with the worst performances (Pd/CNPDs and Pd/NCs). In these cases, the main ceria particle size is almost the same (about 20 nm) and ceria reduction degree are quite similar (both low), therefore difference in activity can be traced back to the different amount of {100} vs {111} facets. Conversely, the two different types of nanorods are structurally very similar (same shape and crystal orientation), but with rather different dimensions. This "size effect" strongly affects the interaction with Pd nanoparticles leading to a different morphology and chemical synergies. Both Pd/SNRs and Pd/LNRs exhibit a high specific surface area (Table 1) due to the small size of ceria particles. These two ceria nanostructures show also the highest concentration of oxygen vacancies and the highest degree of reduction among the as-prepared catalysts. Moreover, they show the highest reducibility associated with the activation process in hydrogen atmosphere, pointing out to a synergistic effect between the metal and the metal oxide support. Indeed it has been reported previously reduced ceria interacts with Pd nanoparticles via reduced species.[51] Nonetheless, Pd nanoparticles must retain a significant level of oxidation to be catalytically active, as documented by previous investigations. In the case of extremely small metal NPs the presence of "activated cationic species" is achieved by an electronic interaction with the substrate and intrinsic size effect as exemplified in the Pd/SNRs system, which exhibits a relevant shift in the BE position of the Pd $3d_{5/2}$ BE from 355.0 eV to 355.9 eV. On the other hand, on larger NPs the same effect can be obtained by a strong chemical interaction with the support that leads to the preservation of a relatively high fraction of oxidized species at the interface. This latter is the case of Pd/LNRs that in reaction conditions maintain the highest amount of Pd(II) and Pd(IV) species.

CONCLUSIONS

In this study we have investigated different types of powder model systems in order to identify which are the most important factors controlling the catalytic activity of Pd/CeO_2 nanocomposites in the decomposition of methanol.

Using a combination of microscopic and spectroscopic techniques we have fully investigated and compared with each other, systems with different shapes (cubes vs rods) dimension (small and long nanorods) and crystallographic orientations (100 vs 111) and in presence and absence of active phase (i.e. Pd).

A systematic analysis combined with measurements of the catalytic activity has allowed to rationalize the origin of the excellent catalytic activity observed in our catalysts and the reason for their differences.

All the catalysts have shown a high methanol conversion and high selectivity toward the production of CO and H_2, however Pd supported on CeO_2 SNRs was by far the best performing system, exhibiting the lowest methanol conversion T_{50} (150°C), which is one the best results ever reported in the literature.

A systematic use of *in situ* XPS has been critical to the comprehension of the surface chemistry of the materials.

In particular photoemission measurement taken at every single step of the catalytic cycle (as prepared catalyst, after activation and after chemical work), has highlighted that the catalyst performances improve (lower T_{50}) with the increase of the Pd-CeO_2 interaction, which favors a higher reducibility of CeO_2 surface as well as the preservation of relatively oxidized palladium species that are the most active site in the catalytic process. This higher reducibility of the oxide

support seems related to the reduction of the ceria particles size and to the increase of their morphological defectivity. On the other hand, the presence of highly reactive Pd NPs is also another factor promoting the reduction of the substrate itself. This highlights to the importance of synergistic effects in nanocatalysis. Notably, the synthesis of the best performing materials was performed at RT and without the use of organic solvents or surfactants, satisfying green chemistry protocols.

ASSOCIATED CONTENT

Supporting Information. Size-dispersion analysis of the nanoparticles, HR-TEM micrographs of the catalysts, Ce3d and Pd3d photoemission lines, as well as the separations into single chemical components, of the Pd decorated catalysts and of bare ceria nanostructures.

The following files are available free of charge.

Supporting Information (PDF)

AUTHOR INFORMATION

Corresponding Author

* Email: stefano.agnoli@unipd.it

Author Contributions

The manuscript was written through contributions of all authors. All authors have given approval to the final version of the manuscript.

Funding Sources

Any funds used to support the research of the manuscript should be placed here (per journal style).

ACKNOWLEDGMENT

Financial support by the University of Padova through the grant “Attrezzature scientifche fnalizzate alla ricerca – Bando 2012” is acknowledged.

REFERENCES

[1] Spivey J. J. Catalysis in the development of clean energy technologies. *Catal. Today*, **2004**, *100*(1-2), 171-180.

[2] Zhang Q.; Liu G.; Wang L.; Zhang X.; Li G. Controllable Decomposition of Methanol for Active Fuel Cooling Technology. *Energy Fuels* **2014**, *28*, 4431−4439.

[3] Kapoor M.P.; Ichihashi Y.; Kuraoka K.; Shen W-J.; Matsamura Y. Catalytic Methanol Decomposition Over Palladium Deposited on Mesoporous Cerium Oxide. *Catalysis letters*, **2003**, *88*, 83-87.

[4] Cheng W.H. Development of Methanol Decomposition Catalysts for Production of H2 and CO. *Acc. Chem. Res*., **1999**, *32*, 685.

[5] Yamada Y.; Tsung C.K.; Huang W.; Huo Z.; Soejima T.; Aliaga C.E.; Somorjai G.A.; Yang P. Nanocrystal bilayer for tandem catalysis. *Nat. Chem.*, **2011**, *3(5)*, 372-6.

[6] Su J.; Xie C.; Chen C.; Yu Y.; Kennedy G.; Somorjai G. A.; Yang P. Insights into the Mechanism of Tandem Alkene Hydroformylation over a Nanostructured Catalyst with Multiple Interfaces. *J. Am. Chem. Soc.*, **2016**, *138*, 11568-11574.

[7] Huang W.; Gao Y. Morphology-dependent surface chemistry and catalysis of CeO2 nanocrystals. *Catal. Sci. Technol*., **2014**, *4*, 3772-3784

[8] Montini T.; Melchionna M.; Monai M.; Fornasiero P. Fundamentals and Catalytic Applications of CeO2-Based Materials. *Chem. Rev.*, **2016**, *116*, 5987−6041.

[9] Qiao Z.-A.; W. Zili; Dai S. Shape-Controlled Ceria-based Nanostructures for Catalysis Applications. *ChemSusChem*, **2013**, *6*, 1821 – 1833.

[10] Hu Z.; Liu X.; Meng D.; Guo Y.; Guo Y.; Lu G. Effect of Ceria Crystal Plane on the Physicochemical and Catalytic Properties of Pd/Ceria for CO and Propane Oxidation *ACS Catal.* **2016**, *6*, 2265−2279.

[11] Si R.; Flytzani-Stephanopoulos M. Shape and Crystal-Plane Effects of Nanoscale Ceria on the Activity of Au-CeO2 Catalysts for the Water–Gas Shift Reaction. *Angew. Chem. Int. Ed.*, **2008**, *47*, 2884 –2887.

[12] Fan L.; Fujimoto K. Reaction Mechanism of Methanol Synthesis from Carbon Dioxide and Hydrogen on Ceria-Supported Palladium Catalysts with SMSI Effect. *J. Catal.* ,**1997**, *172*, 238

[13] Liu Y.; Hayakawa T.; Ishii T.; Kumagai M.; Yasuda H.; Suzuki K.; Hamakawa S.; Murata K. Methanol decomposition to synthesis gas at low temperature over palladium supported on ceria–zirconia solid solutions. *Applied Catalysis A: General*, **2001**, *210*, 301-314.

[14] Matsumura Y.; Shen W. J. Methanol Decomposition and Synthesis Over Palladium Catalysts. Topics in Catalysis, **2003**, 22, 3-4.

[15] Davis, J.L.; Barteau, M.A. Spectroscopic identification of alkoxide, aldehyde, and acyl intermediates in alcohol decomposition on Pd(111) *Surf. Sci.* **1990**, 235 235.

[16] Levis, R.J.; Zhicheng, J.; Winograd, N. Thermal decomposition of methanol absorbed on palladium{111}. A new reaction pathway involving methyl formation *J. Am. Chem. Soc.* 1989, *111*, 4605.

[17] Kaichev, V.V.; Miller, A.V.; Prosvirin, I.P.; Bukhtiyarov V.I. In situ XPS and MS study of methanol decomposition and oxidation on Pd(111) under millibar pressure range *Surf. Sci.* **2012**, *606*, 420-425.

[18] Morkel, M.; Kaichev, V. V.; Rupprechter, G.; Freund, H.-J.; Prosvirin, I. P.; Bukhtiyarov V. I. Methanol Dehydrogenation and Formation of Carbonaceous Overlayers on Pd(111) Studied by High-Pressure SFG and XPS Spectroscopy *J. Phys. Chem. B*, **2004**, *108*, 12955–12961

[19] Shen W-J-; Matsumura,Y. Low-temperature methanol decomposition to carbon monoxide and hydrogen catalysed over cationic palladium species in Pd/CeO_2. *Phys. Chem. Chem. Phys*., **2000**, *2*, 1519-1522.

[20] Artiglia L.; Orlando F.; Roy K.; Kopelent R.; Safonova O.; Nachtegaal M.; Huthwelker T.; van Bokhoven J.A. Introducing. Time Resolution to Detect Ce^{3+} Catalytically Active Sites at the Pt/CeO_2 Interface through Ambient Pressure X-Ray Photoelectron. Spectroscopy. *J. Phys. Chem. Lett.*, **2017**, *8*, 102−108.

[21] Tan H.; Wang J.; Yu S.; Zhou K. Support Morphology-Dependent Catalytic Activity of Pd/CeO2 for Formaldehyde Oxidation *Environ. Sci. Technol*., **2015**, *49*, 8675−8682.

[22] Mullins D.R. The surface chemistry of cerium oxide. *Surface Science Reports*, **2015**, *70*, 42-85

[23] Wu Z.; Li M.; Mullins D.R.; Overbury S. H. Probing the Surface Sites of CeO2 Nanocrystals with Well-Defined Surface Planes via Methanol Adsorption and Desorption. *ACS Catal*., **2012**, *2*, 2224-2234.

[24] Trovarelli A.; Llorca J. Ceria Catalysts at Nanoscale: How Do Crystal Shapes Shape Catalysis? *ACS Catal.*, **2017**, *7*, 4716-4735.

[25] Zabilskiy M.; Djinović P.; Tchernychova E.; Tkachenko O. P.; Kustov L. M.; Pintar A. Nanoshaped CuO/CeO2 Materials: Effect of the Exposed Ceria Surfaces on Catalytic Activity in N2O Decomposition Reaction. *ACS Catal.*, **2015**, *5*, 5357−5365.

[26] Araiza D.G.; Gómez-Cortés A.; Díaz G. Partial oxidation of methanol over copper supported on nanoshaped ceria for hydrogen production. Catal. Today **2017**, *282*, 185-194.

[27] Ma Z.; Zhao S.; Pei X.; Xiong X.; Hu B. New insights into the support morphology-dependent ammonia synthesis activity of Ru/CeO2 catalysts. *Catal. Sci. Technol*., **2017**, *7*, 191.

[28] Wang N.; Qian W.; Chu W.; Wei F. Crystal-plane effect of nanoscale CeO2 on the catalytic performance of Ni/CeO2 catalysts for methane dry reforming. *Catal. Sci. Technol.*, **2016**, *6*, 3594.

[29] Araiza D. G.; Gómez-Cortés A.; Díaz G. Reactivity of methanol over copper supported on well-shaped CeO2: a TPD-DRIFTS study. *Catal. Sci. Technol.*, **2017**, *7*, 5224.

[30] Usami Y.; Kagawa K.; Kawazoe M.; Matsumura Y.; Sakurai H.; Haruta M. Preparation of Pd/CeO2 Catalyst for Methanol Decomposition *Stud. Surf. Sci. Catal.*, **1998**, *118*, 83.

[31] Shen W-J.; Okumura M.; Matsumura Y.; Haruta M. The influence of the support on the activity and selectivity of Pd in CO hydrogenation. *Appl. Catal. A*, **2001**, *213*, 225.

[32] Imamura S.; Higashihara T.; Saito Y.; Aritani H.; Kanai H.; Matsumura Y.; Tsuda N. Decomposition of Methanol on Pt-loaded Ceria. *Catal. Today*, **1999**, *50*, 369-380.

[33] Pan C.; Zhang D.; Shi L.; Fang J. Template-Free Synthesis, Controlled Conversion, and CO Oxidation Properties of CeO2 Nanorods, Nanotubes, Nanowires, and Nanocubes. *Eur. J. Inorg. Chem.*, **2008**, *15*, 2429–2436.

[34] Mai H. X.; Sun L. D.; Zhang Y. W.; Si R.; Feng W.; Zhang H. P.; H. Liu C.; Yan C. H. J. Shape-selective synthesis and oxygen storage behavior of ceria nanopolyhedra, nanorods, and nanocubes. *J. Phys. Chem. B*, **2005**, *109*, 24380−24385.

[35] Graham G. W.; Weber W. H.; Peters C. R.; Usmen R. Empirical method for determining CeO2-particle size in catalysts by raman spectroscopy. *J. Catal.*, **1991**, *130*, 310-313.

[36] Lee Y.; He G.; Akey A. J.; Si R.; Flytzani-Stephanopoulos M.; Herman I. P. Raman Analysis of Mode Softening in Nanoparticle CeO2−δ and Au-CeO2−δ during CO Oxidation. *J. Am. Chem. Soc.*, **2011**, *133*, 12952.

[37] Oh S.-H.; Hoflund G. B. Chemical State Study of Palladium Powder and Ceria-Supported Palladium during Low-Temperature CO Oxidation. *J. Phys,Chem. A*, **2006**, *110*, 7609

[38] Matsumura Y.; Okumura M.; Usami Y.; Kagawa K.; Yamashita H.; Anpo M.; Haruta M. Low-temperature decomposition of methanol to carbon monoxide and hydrogen with low activation energy over Pd/ZrO2 catalyst. Catal. Lett. **1997**, *44*, 189-191

[39] Burroughs P.; Hamnett A.; Orchard A. F.; Thornton G. Satellite structure in the X-ray photoelectron spectra of some binary and mixed oxides of lanthanum and cerium. *J. Chem. Soc., Dalton Trans.*, **1976**, *17*, 1686−1698.

[40] Skála T.; Šutara F.; Škoda M.; Prince K C.; Matolín V. Palladium interaction with CeO(2), Sn-Ce-O and Ga-Ce-O layers. *J. Phys. Condens. Matter*, **2008**, *21*, 055005.

[41] Matolín V.; Matolínová I.; Sedláček L.; Prince K. C.; Skála T. A resonant photoemission applied to cerium oxide based nanocrystals. *Nanotechnology* **2009**, *20*, 215706.

[42] Artiglia L.; Agnoli S.; Paganini M. C.; Cattelan M.; Granozzi G. TiO2@CeOx core-shell nanoparticles as artificial enzymes with peroxidase-like activity. *ACS Appl. Mater. Interfaces*, **2014**, *6*, 20130.

[43] Song J.; Rodenbough P. P.; Xu W.; Senanayake S. D.; Chan S.-W. Reduction of Nano-Cu2O: Crystallite Size Dependent and the Effect of Nano-Ceria Support. *J. Phys. Chem. C*, **2015**, *119*, 17667-17672.

[44] Congting S.; Xue D. Size-dependent oxygen storage ability of nano-sized ceria. *Phys. Chem. Chem. Phys.* **2013,** *15*, 14414-14419.

[45] Shen W-J.; Matsumura Y. Interaction between palladium and the support in Pd/CeO2 prepared by deposition–precipitation method and the catalytic activity for methanol decomposition. *J. Mol. Catal. A: Chem.*, **2000**, *153*, 165-168.

[46] S Hüfner.; Wertheim G. K.; Buchanan D. N. E. Title: X-ray photoemission spectra of palladium. *Chem. Phys. Lett.*, **1974**, *24*, 527.

[47] Rao C. N. R.; Kulkarni G. U.; Thomas P. J.; Edwards P. P. Size-Dependent Chemistry: Properties of Nanocrystals. *Chem.-Eur. J.*, **2002**, *8*, 28.

[48] Favaro M.; Agnoli S.; Perini L.; Durante C.; Gennaro A.; Granozzi G. Palladium nanoparticles supported on nitrogen-doped HOPG: a surface science and electrochemical study. *Phys. Chem. Chem. Phys*., **2013**, *15*, 2923.

[49] Vannice M.A.; Sudhakar C.; Freeman M. Methanol and methane formation over palladium dispersed on the lanthanide rare earth oxides. *J. Catal.,* **1987,** *108*, 97.

[50] Diagne C.; Idriss H.; Pepin I.; Hindermann J.P.; Kiennemann A. Temperature-programmed desorption studies on Pd/CeO2 after methanol and formic acid adsorption and carbon monoxide—hydrogen reaction. *Appl. Catal.,* **1989,** *50*, 43-53.

[51] Monteiro R. de S.; Noronha F. B.; Diegue L. C.; Schmal M. Characterization of Pd-CeO2 interaction on alumina support and hydrogenation of 1,3-butadiene. *Appl. Catal. A: Gen.,* **1995**, *131*, 89.